in vitro studies (*26*, *36*, *38*). However, at which specific step the inhibitory action of NAC on ER targeting is counteracted by the SRP pathway is unclear.

NAC is evolutionarily conserved from yeast to man and is essential in eukaryotes, except for yeast (*13*, *30*, *39*, *40*). Knockdown of α-NAC in human HeLa S3 cells also activates ER stress responses and causes mitochondrial dysfunction (*41*). Thus, the function of NAC as an ER targeting inhibitor appears to be well conserved during evolution, at least from *C. elegans* to mammalians. Recent studies showed that NAC is sequestered by cytosolic aggregates under protein folding stress conditions (*18*, *42*). This raises the question whether proteotoxic stress in the cytoplasm causes dysfunction of NAC, leading to incorrect sorting of proteins to the ER and mitochondria. A link between cytosolic protein aggregation and ER stress is well established (*43*), and it will be interesting to investigate the role of NAC in this context.

REFERENCES AND NOTES

1. M. Halic *et al.*, *Nature* **427**, 808–814 (2004).
2. M. Halic *et al.*, *Science* **312**, 745–747 (2006).
3. Y. Nyathi, B. M. Wilkinson, M. R. Pool, *Biochim. Biophys. Acta* **1833**, 2392–2402 (2013).
4. T. A. Rapoport, *Nature* **450**, 663–669 (2007).
5. T. Schwartz, G. Blobel, *Cell* **112**, 793–803 (2003).
6. P. Walter, I. Ibrahimi, G. Blobel, *J. Cell Biol.* **91**, 545–550 (1981).
7. B. Wiedmann, H. Sakai, T. A. Davis, M. Wiedmann, *Nature* **370**, 434–440 (1994).
8. N. Borgese, W. Mok, G. Kreibich, D. D. Sabatini, *J. Mol. Biol.* **88**, 559–580 (1974).
9. B. Jungnickel, T. A. Rapoport, *Cell* **82**, 261–270 (1995).
10. K. U. Kalies, D. Görlich, T. A. Rapoport, *J. Cell Biol.* **126**, 925–934 (1994).
11. B. Lauring, H. Sakai, G. Kreibich, M. Wiedmann, *Proc. Natl. Acad. Sci. U.S.A.* **92**, 5411–5415 (1995).
12. A. Prinz, E. Hartmann, K. U. Kalies, *Biol. Chem.* **381**, 1025–1029 (2000).
13. T. A. Bloss, E. S. Witze, J. H. Rothman, *Nature* **424**, 1066–1071 (2003).
14. S. L. Rea, D. Wu, J. R. Cypser, J. W. Vaupel, T. E. Johnson, *Nat. Genet.* **37**, 894–898 (2005).
15. Materials and methods are available as supplementary materials on *Science* Online.
16. M. Calfon *et al.*, *Nature* **415**, 92–96 (2002).
17. T. Yoneda *et al.*, *J. Cell Sci.* **117**, 4055–4066 (2004).
18. J. Kirstein-Miles, A. Scior, E. Deuerling, R. I. Morimoto, *EMBO J.* **32**, 1451–1468 (2013).
19. M. R. Adelman, D. D. Sabatini, G. Blobel, *J. Cell Biol.* **56**, 206–229 (1973).
20. S. S. Vembar, J. L. Brodsky, *Nat. Rev. Mol. Cell Biol.* **9**, 944–957 (2008).
21. F. Urano *et al.*, *J. Cell Biol.* **158**, 639–646 (2002).
22. F. Schwarz, M. Aebi, *Curr. Opin. Struct. Biol.* **21**, 576–582 (2011).
23. S. Cabantous, T. C. Terwilliger, G. S. Waldo, *Nat. Biotechnol.* **23**, 102–107 (2005).
24. W. Neupert, J. M. Herrmann, *Annu. Rev. Biochem.* **76**, 723–749 (2007).
25. O. Yogev, O. Pines, *Biochim. Biophys. Acta* **1808**, 1012–1020 (2011).
26. I. Möller *et al.*, *Proc. Natl. Acad. Sci. U.S.A.* **95**, 13425–13430 (1998).
27. A. Neuhof, M. M. Rolls, B. Jungnickel, K. U. Kalies, T. A. Rapoport, *Mol. Biol. Cell* **9**, 103–115 (1998).
28. D. Raden, R. Gilmore, *Mol. Biol. Cell* **9**, 117–130 (1998).
29. M. del Alamo *et al.*, *PLOS Biol.* **9**, e1001100 (2011).
30. B. Reimann *et al.*, *Yeast* **15**, 397–407 (1999).
31. T. Ast, G. Cohen, M. Schuldiner, *Cell* **152**, 1134–1145 (2013).
32. S. C. Mutka, P. Walter, *Mol. Biol. Cell* **12**, 577–588 (2001).
33. R. M. Voorhees, I. S. Fernández, S. H. Scheres, R. S. Hegde, *Cell* **157**, 1632–1643 (2014).
34. R. D. Wegrzyn *et al.*, *J. Biol. Chem.* **281**, 2847–2857 (2006).
35. M. Pech, T. Spreter, R. Beckmann, B. Beatrix, *J. Biol. Chem.* **285**, 19679–19687 (2010).
36. Y. Zhang *et al.*, *Mol. Biol. Cell* **23**, 3027–3040 (2012).
37. U. Raue, S. Oellerer, S. Rospert, *J. Biol. Chem.* **282**, 7809–7816 (2007).
38. T. Powers, P. Walter, *Curr. Biol.* **6**, 331–338 (1996).
39. J. M. Deng, R. R. Behringer, *Transgenic Res.* **4**, 264–269 (1995).
40. D. C. Markesich, K. M. Gajewski, M. E. Nazimiec, K. Beckingham, *Development* **127**, 559–572 (2000).
41. Y. Hotokezaka *et al.*, *Cell Death Differ.* **16**, 1505–1514 (2009).
42. H. Olzscha *et al.*, *Cell* **144**, 67–78 (2011).
43. R. V. Rao, D. E. Bredesen, *Curr. Opin. Cell Biol.* **16**, 653–662 (2004).

ACKNOWLEDGMENTS

We gratefully acknowledge the help of A. Dillin and K. Steffen to get started with this *C. elegans* project. We thank the *Caenorhabditis* Genetics Center for strains and E. Schulze for the microinjection training. We also thank A. Page, W. Neupert, and C. Bargmann for providing reagents. We thank R. Schloemer, K. Turgay, C. Schlatterer, S. Zboron, and E. Oberer-Bley for their critical discussions and valuable help with the manuscript. This work was supported by research grants from the German Science Foundation (DFG; SFB969/A01) and from Human Frontier in Science Program (HFSP; RGP025) to E.D. Data are deposited in Gene Expression Omnibus under accession no. GSE63928.

SUPPLEMENTARY MATERIALS

www.sciencemag.org/content/348/6231/201/suppl/DC1
Materials and Methods
Figs. S1 to S7
References (*44*–*48*)

19 December 2014; accepted 13 February 2015
10.1126/science.aaa5335

REPORTS

QUANTUM GASES

Experimental observation of a generalized Gibbs ensemble

Tim Langen,[1] Sebastian Erne,[1,2,3] Remi Geiger,[1] Bernhard Rauer,[1] Thomas Schweigler,[1] Maximilian Kuhnert,[1] Wolfgang Rohringer,[1] Igor E. Mazets,[1,4,5] Thomas Gasenzer,[2,3] Jörg Schmiedmayer[1]*

The description of the non-equilibrium dynamics of isolated quantum many-body systems within the framework of statistical mechanics is a fundamental open question. Conventional thermodynamical ensembles fail to describe the large class of systems that exhibit nontrivial conserved quantities, and generalized ensembles have been predicted to maximize entropy in these systems. We show experimentally that a degenerate one-dimensional Bose gas relaxes to a state that can be described by such a generalized ensemble. This is verified through a detailed study of correlation functions up to 10th order. The applicability of the generalized ensemble description for isolated quantum many-body systems points to a natural emergence of classical statistical properties from the microscopic unitary quantum evolution.

Information theory provides powerful concepts for statistical mechanics and quantum many-body physics. In particular, the principle of entropy maximization (*1*–*3*) leads to the well-known thermodynamical ensembles, which are fundamentally constrained by conserved quantities such as energy or particle number (*4*). However, physical systems can contain many additional conserved quantities, which raises the question of whether there exists a more general statistical description for the steady states of quantum many-body systems (*5*).

Specifically, the presence of nontrivial conserved quantities puts constraints on the available phase space of a system, which strongly affects the dynamics (*6*–*9*) and inhibits thermalization (*10*–*12*). Instead of relaxing to steady states described by the usual thermodynamical ensembles, a generalized Gibbs ensemble (GGE) was proposed to describe the corresponding steady states via the many-body density matrix

$$\hat{\rho} = \frac{1}{Z}\exp\left(-\sum_m \lambda_m \hat{\mathcal{I}}_m\right) \qquad (1)$$

(*3*, *11*, *13*, *14*), where $\hat{\mathcal{I}}_m$ denotes a set of conserved quantities and $Z = \mathrm{Tr}[\exp(-\sum_m \lambda_m \hat{\mathcal{I}}_m)]$ is the partition function. The Lagrange multipliers λ_m associated with the conserved quantities are obtained by maximization of the entropy under the condition that the expectation values of the conserved quantities are fixed to their initial values. The emergence of such a maximum-entropy state does not contradict a unitary evolution according to quantum mechanics. Rather, it reflects that the true quantum state is indistinguishable from the maximum-entropy ensemble with respect to a set of sufficiently local observables (*5*).

[1]Vienna Center for Quantum Science and Technology, Atominstitut, TU Wien, 1020 Vienna, Austria. [2]Institut für Theoretische Physik, Ruprecht-Karls-Universität Heidelberg, 69120 Heidelberg, Germany. [3]ExtreMe Matter Institute (EMMI), GSI Helmholtzzentrum für Schwerionenforschung GmbH, 64291 Darmstadt, Germany. [4]Wolfgang Pauli Institute, 1090 Vienna, Austria. [5]Ioffe Physico-Technical Institute, 194021 St. Petersburg, Russia.
***Corresponding author. E-mail: schmiedmayer@atomchip.org**

The GGE is a direct generalization of the usual thermodynamical ensembles and is formally capable of describing a wide range of dynamically emerging steady states (*15*). For example, in the case where only the energy is conserved, the GGE reduces to the standard canonical or Gibbs ensemble, with temperature being the only Lagrange multiplier (*4*). Moreover, the GGE famously provides a description for the steady states of

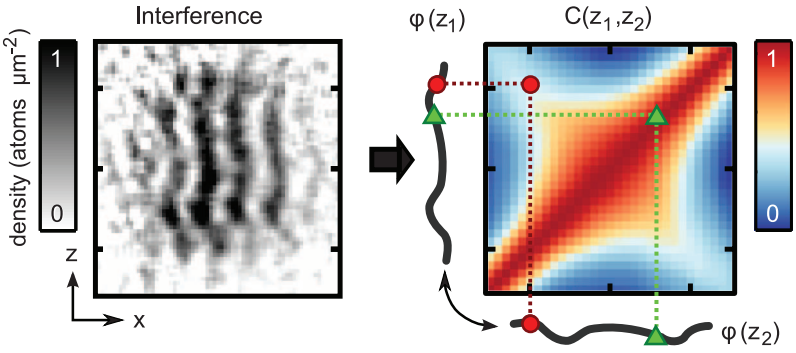

Fig. 1. Experimental concept. A non-equilibrium system is prepared by splitting a 1D Bose gas into two halves. After an evolution time t, matter-wave interference is used to extract the local relative phase profile $\varphi(z)$ between the two halves. This is accomplished by measuring the local position of the fluctuating interference fringes. Subsequently, the phase profile is used to calculate the two-point correlation function $C(z_1, z_2) \sim \langle \exp[i\varphi(z_1) - i\varphi(z_2)] \rangle$ as a function of all possible coordinates z_1 and z_2 along the length of the measured phase profile. For $z_1 = z_2$ (e.g., green triangle on the diagonal), $C(z_1, z_2) = 1$. Coordinates with $z_1 = -z_2$ (e.g., red point) are located symmetrically around the center of the system and are found on the antidiagonal of the correlation function.

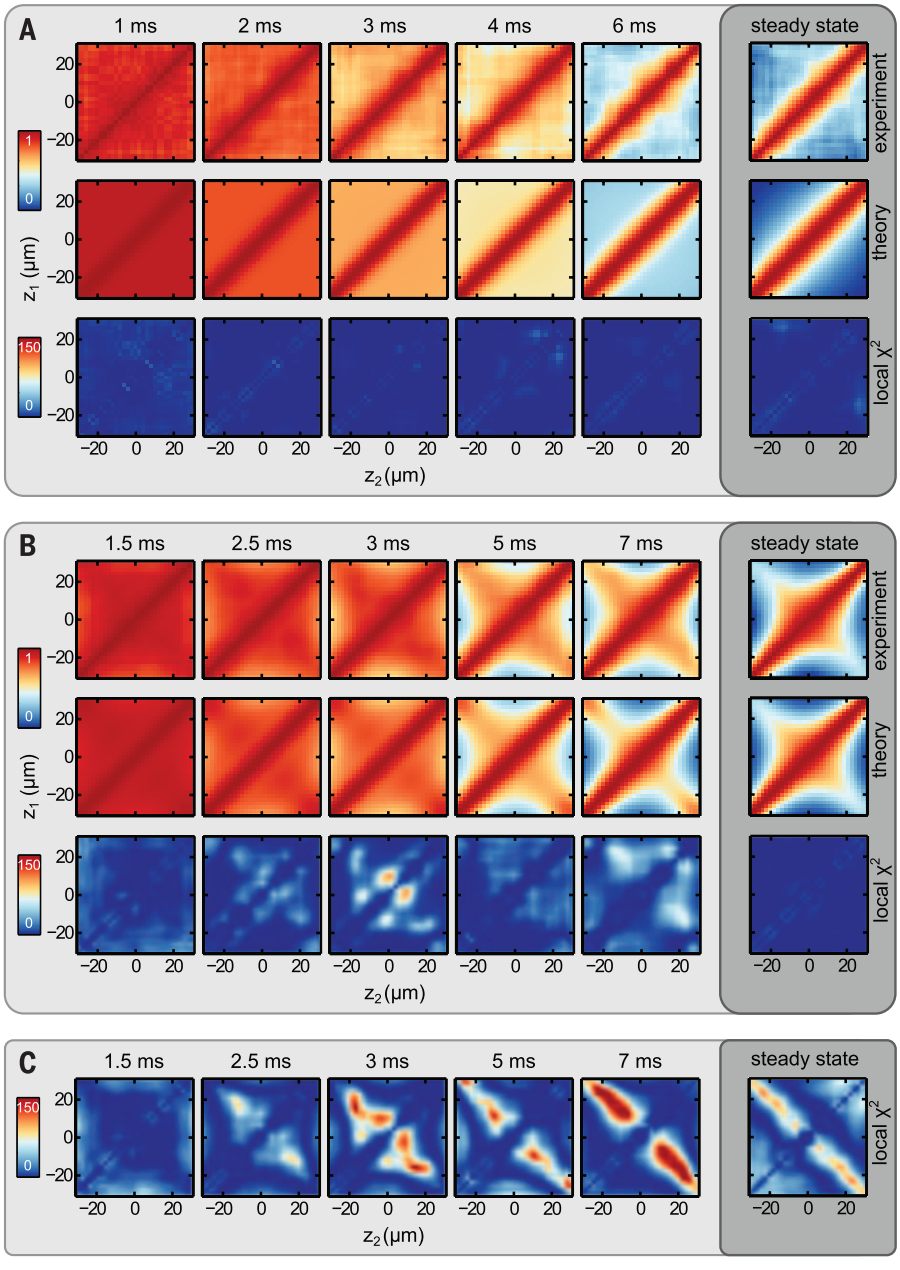

Fig. 2. Two-point phase correlation functions $C(z_1, z_2)$ for increasing evolution time. (**A** and **B**) Different initial states were prepared using two different splitting protocols. Both states show a characteristic maximum on the diagonal and a decay of correlations away from the diagonal. We used a χ^2 analysis to quantify the agreement of our theoretical model and the experiments. The steady state and the dynamics in (A) can be well described by a single temperature T_{eff}. (**C**) The single-temperature model fails for the steady state and the dynamics in (B), which require more temperatures to explain additional correlations on the antidiagonal (see text). The observation of different temperatures in the same steady state constitutes our observation of a GGE. The center of the system is located at $z_1 = z_2 = 0$; color marks the amount of correlations between 0 and 1 and the local χ^2 contribution between 0 and 150. The uncertainty of the correlation functions is estimated via bootstrapping over approximately 150 experimental realizations (*25*).

integrable systems, which have as many independent conserved quantities as they have degrees of freedom (*9*, *11*, *14*). Even if quantities are only approximately conserved, the GGE description was formally shown to be valid for extended time scales (*16*). The GGE has also been suggested as a description for many-body localized states (*17*). Numerical evidence for the emergence of a GGE has been provided for many systems, but a direct experimental observation has been lacking.

Here, we experimentally studied the relaxation of a trapped one-dimensional (1D) Bose gas. Our system is a close realization of the Lieb-Liniger model describing a homogeneous gas of 1D bosons with contact interactions, which is one of the prototypical examples of an integrable system (*18*, *19*). In the thermodynamic limit, its exact Bethe Ansatz solutions imply an infinite number of conserved quantities, which provides a memory of an initial non-equilibrium state, forcing the gas to relax to a GGE. Recent results have also shown that trapped 1D Bose gases can be approximately integrable over very long time scales, enabling the detailed investigation of integrable dynamics (*6*, *7*, *10*, *20*, *21*). To demonstrate the emergence of a GGE, we prepared such a 1D Bose gas in different initial non-equilibrium states and observed how they each relaxed to steady states that maximize entropy according to the initial values of the conserved quantities.

The experiments started with a phase-fluctuating 1D Bose gas (*22*) of ^{87}Rb atoms that was prepared and trapped using an atom chip (*23*). We initialized the non-equilibrium dynamics by transversally splitting this single 1D gas coherently into two nominally identical 1D systems, each containing half of the atoms on average. Information about the total system was extracted using matter-wave interferometry between the two halves (*6*, *20*, *21*, *24*). This enabled the time-resolved measurement of individual two-point and higher-order N-point phase correlation functions,

$$C(z_1, z_2, ..., z_N) \sim \langle \Psi_1(z_1)\Psi_2^\dagger(z_1)\Psi_1^\dagger(z_2)\Psi_2(z_2)...\Psi_1^\dagger(z_N)\Psi_2(z_N)\rangle \sim \langle \exp[i\varphi(z_1) - i\varphi(z_2) + ... - i\varphi(z_N)]\rangle \quad (2)$$

where z_1, z_2, ..., z_N are N coordinates along the length of the system, and $\varphi(z)$ is the relative phase between the two halves (*25*). As described below, these correlation functions reveal detailed information about the dynamics and the steady states of the system.

We start with the two-point correlation function $C(z_1, z_2) \sim \langle \exp[i\varphi(z_1) - i\varphi(z_2)]\rangle$. Previously, this correlation function was studied in regions where the system is approximately translationally invariant (*21*, *26*), that is, $C(z_1, z_2) \equiv C(z_1 - z_2)$. Here, more comprehensive information about generic many-body states is obtained by mapping the full correlation function $C(z_1, z_2)$ for any combination of the coordinates z_1 and z_2 (Fig. 1).

Our observations after a typical splitting, which is fast relative to the dynamics of the system and therefore realizes a quench (*25*), are summarized in Fig. 2A. As every point in the system is perfectly correlated with itself, the correlation functions exhibit a maximum on the diagonal $z_1 = z_2$ for all times. Away from the diagonal, the system shows a light cone–like decay of correlations (*21*) leading to a steady state. From a theoretical point of view, the emergence of this steady state is a consequence of prethermalization (*6*, *27*–*31*), which in the present case can be described as the dephasing of phononic excitations (*29*, *31*–*33*). The occupation numbers n_m of these excitations are the conserved quantities of the corresponding integrable model (*25*).

With a knowledge of the conserved quantities, we can directly calculate the Lagrange multipliers λ_m for the GGE. In terms of the excitation energies ε_m they can be written as $\lambda_m = \beta_m\varepsilon_m$, which defines an effective temperature $1/\beta_m$ for every excitation mode.

For the steady state illustrated in Fig. 2A, the proportionality factor β_m can be well described by $\beta_m \approx \beta_{eff} = 1/k_B T_{eff}$ (where k_B is the Boltzmann constant). A fit yields $k_B T_{eff} = 0.50$ (±0.01) × μ, which is independent of m and in very good agreement with theory (*6*, *33*). Here, μ denotes the chemical potential in each half of the system. Although it is a GGE in principle, for our experiment (which observes the relative phase between the two halves of the system) it becomes formally equivalent to the usual Gibbs ensemble with a single temperature T_{eff} (*25*).

To obtain direct experimental signatures of a genuine GGE, we modified the initial state so that it exhibited different temperatures for different excitation modes. This was accomplished by changing the ramp that splits the initial gas into two halves (*25*). The results are shown in Fig. 2B. In addition to the maximum of correlations on the diagonal, a pronounced second maximum on the antidiagonal can be seen. This corresponds to enhanced correlations of the points $z_1 = -z_2$, which are located symmetrically around the center of the system. These correlations are a direct consequence of an increased population of quasi-particle modes that are even, and a decreased population of quasi-particle modes that are odd, under a mirror reflection with respect to the longitudinal trap center. Consequently, the observations can be described to a first approximation by the above theoretical model but with different temperatures—that is, with $\beta_{2m} = 1/[k_B(T_{eff} + \Delta T)]$ for the even modes and $\beta_{2m-1} = 1/[k_B(T_{eff} - \Delta T)]$ for the odd modes, respectively. Fitting the experimental data of the steady state with this model, we find $k_B T_{eff} = 0.64$ (±0.01) × μ, $\Delta T = 0.48$ (±0.01) × T_{eff}, and a reduced $\chi^2 \approx 6$.

More detailed insights and a more accurate description of the experimental data can be gained by fitting the steady state with the individual mode occupations as free parameters. The results yield a reduced χ^2 close to 1 and thus

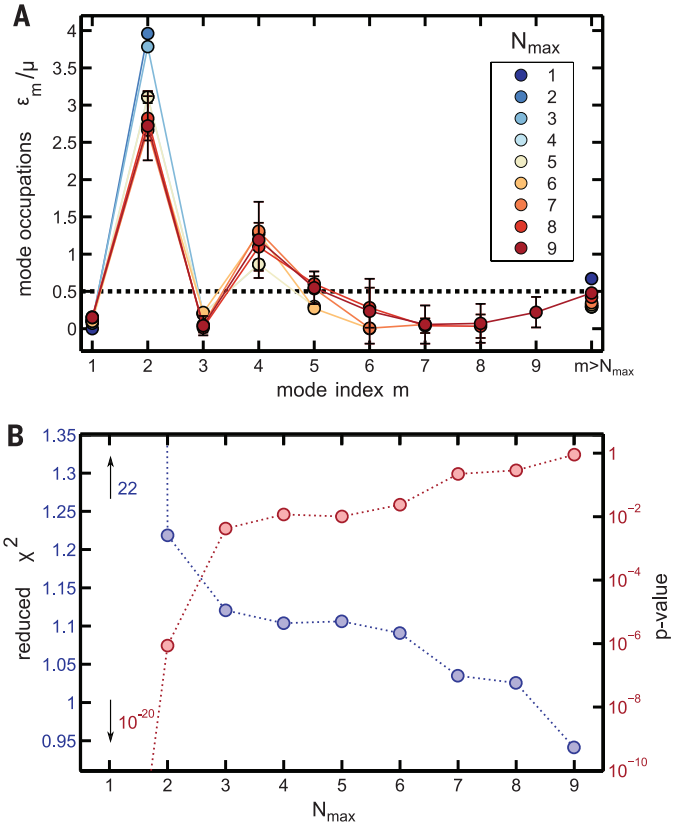

Fig. 3. Statistical analysis of the fitting procedure. (**A**) Occupation numbers n_m (in units of ε_m/μ) of the quasi-particle modes with index m, for different fitting procedures applied to the data from Fig. 2B. The color of the points encodes results where modes up to $m = N_{max}$ are fitted freely, whereas all higher modes are fit with the same occupation number. The plot reveals that the occupation of the lowest even modes is increased, and that of the lowest odd modes is decreased, relative to the single-temperature state from Fig. 2A (dashed line). (**B**) Scaling of the reduced χ^2 value, and of the corresponding P value with N_{max}. The occupation numbers of the lowest nine modes and a single occupation number for all higher modes are sufficient to describe the experimental data to very good accuracy.

a very good description of the experimental data (see Fig. 2B). As expected from our intuitive two-temperature model, the fitting confirms that the occupation of even modes is strongly enhanced, whereas the occupation of odd modes is reduced (see Fig. 3A). Fixing these occupation numbers extracted from the steady state, our theoretical model also describes the complete dynamics very well. This clearly demonstrates that the different populations of the modes were imprinted onto the system by the splitting quench and are conserved during the dynamics. In contrast, a simple model based on a usual Gibbs ensemble with just one temperature for all modes clearly fails to describe the data [best fit: $k_B T_{eff}$ = 0.38 (±0.01) × μ, reduced $\chi^2 \approx 25$], as visualized in Fig. 2C.

Notably, our fitting results for the GGE exhibit strong correlations between the different even modes and the different odd modes, respectively. This demonstrates the difficulty in fully and independently determining the parameters of such complex many-body states. In fact, any full tomography of all parameters would require exponentially many measurements. The results thus clearly show the presence of a GGE with at least two, but most likely many more temperatures.

Our work raises the interesting question of how many Lagrange multipliers are needed in general to describe the steady state of a realistic integrable quantum system. In analogy to classical mechanics, where N conserved quantities exist for a generic integrable system with N degrees of freedom, integrability in quantum many-body systems has been proposed to be characterized by the fact that the number of independent local conserved quantities scales with the number of particles (*5*). Here we conjecture that many experimentally obtainable initial states evolve in time into steady states, which can be described to a reasonable precision by far fewer than N Lagrange multipliers (*8*, *34*). This would have the appeal of a strong similarity to thermodynamics, where also only a few parameters are needed to describe the properties of a system on macroscopic scales.

To illustrate this in our specific case, we investigated how many distinct Lagrange multipliers need to be considered in the GGE to describe our data with multiple temperatures (Fig. 3). Including more and more modes in the fitting of the experimental data, we found that the reduced χ^2 values decrease and settle close to unity for nine included modes, with all higher modes being fitted by one additional Lagrange multiplier. Looking at the P value for the measured χ^2 (*35*) shows that only a limited number of Lagrange multipliers needs to be specified to describe the observables under study to the precision of the measurement. A simple numerical estimate based on the decreasing contribution of higher modes to the measured correlation functions and the limited imaging resolution leads to approximately 10 Lagrange multipliers, which is in good agreement with our observations (*25*). Moreover, comparing this result with the single-temperature steady state discussed earlier illustrates that the complexity of the initial state plays an important role for the number of Lagrange multipliers that need to be included in a GGE.

In general, deviations of steady states from the GGE description are expected to manifest first in higher-order correlation functions. To provide further evidence for our theoretical description and the presence of a GGE, Fig. 4 shows examples of measured 4-point, 6-point, and 10-point correlation functions of the steady state. Like the 2-point correlation functions, they are in very good agreement with the theoretical model and clearly reveal the difference between the GGE and the usual Gibbs ensemble. This confirms that the description based on a GGE with the parameters extracted from the 2-point correlation functions also describes many-body observables, at least up to 10th order.

Our results clearly visualize, both experimentally and theoretically, how the unitary evolution of our quantum many-body system connects to a steady state that can be described by a classical statistical ensemble. We expect our measurements of correlation functions to high order to play an

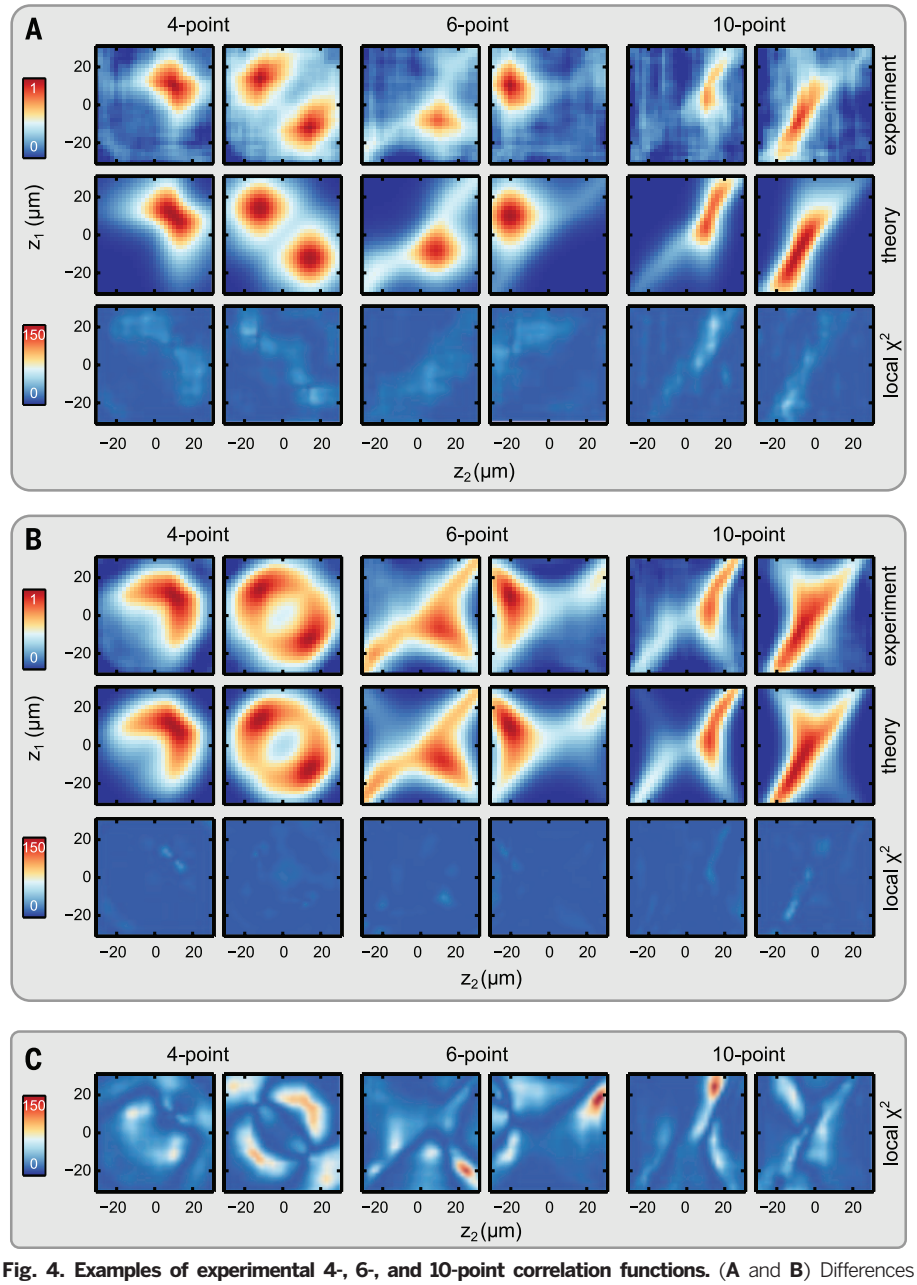

Fig. 4. Examples of experimental 4-, 6-, and 10-point correlation functions. (**A** and **B**) Differences between the steady state described by a single temperature (A) and the steady state described by multiple temperatures (B) are significant and can be captured by the theoretical model. (**C**) The single-temperature model cannot describe the state with multiple temperatures, which is reflected in high values of the local χ^2. From left to right, we plot $C(z_1, 10, z_2, 10)$, $C(z_1, -12, z_2, 14)$, $C(z_1, 10, 10, z_2, -20, 10)$, $C(z_1, -8, 8, z_2, -24, -20)$, $C(z_1, 4, 10, z_2, -8, z_2, -22, -18, 10, -4)$, and $C(z_1, -22, -8, z_2, -22, -26, -22, z_2, -26, -24)$. All coordinates are given in μm and were chosen as representative cases for our high-dimensional data.

important role in new tomography techniques for complex quantum many-body states (*36*). Moreover, the observed tunability of the nonequilibrium states suggests that our splitting process could in the future be used to prepare states tailored for precision metrology (*37*).

REFERENCES AND NOTES

1. C. E. Shannon, W. Weaver, *The Mathematical Theory of Communication* (Univ. of Illinois Press, Urbana, IL, 1949).
2. E. T. Jaynes, *Phys. Rev.* **106**, 620–630 (1957).
3. E. T. Jaynes, *Phys. Rev.* **108**, 171–190 (1957).
4. K. Huang, *Statistical Mechanics* (Wiley, New York, 1987).
5. A. Polkovnikov, K. Sengupta, A. Silva, M. Vengalattore, *Rev. Mod. Phys.* **83**, 863–883 (2011).
6. M. Gring *et al.*, *Science* **337**, 1318–1322 (2012).
7. J. P. Ronzheimer *et al.*, *Phys. Rev. Lett.* **110**, 205301 (2013).
8. J.-S. Caux, F. H. Essler, *Phys. Rev. Lett.* **110**, 257203 (2013).
9. P. Calabrese, F. H. L. Essler, M. Fagotti, *Phys. Rev. Lett.* **106**, 227203 (2011).
10. T. Kinoshita, T. Wenger, D. S. Weiss, *Nature* **440**, 900–903 (2006).
11. M. Rigol, V. Dunjko, V. Yurovsky, M. Olshanii, *Phys. Rev. Lett.* **98**, 050405 (2007).
12. M. Rigol, *Phys. Rev. Lett.* **103**, 100403 (2009).
13. M. A. Cazalilla, *Phys. Rev. Lett.* **97**, 156403 (2006).
14. J.-S. Caux, R. M. Konik, *Phys. Rev. Lett.* **109**, 175301 (2012).
15. M. Rigol, V. Dunjko, M. Olshanii, *Nature* **452**, 854–858 (2008).
16. M. Kollar, F. A. Wolf, M. Eckstein, *Phys. Rev. B* **84**, 054304 (2011).
17. R. Vosk, E. Altman, *Phys. Rev. Lett.* **110**, 067204 (2013).
18. E. H. Lieb, W. Liniger, *Phys. Rev.* **130**, 1605–1616 (1963).
19. V. Korepin, N. Bogoliubov, A. Izergin, *Quantum Inverse Scattering Method and Correlation Functions* (Cambridge Univ. Press, Cambridge, 1993).
20. M. Kuhnert *et al.*, *Phys. Rev. Lett.* **110**, 090405 (2013).
21. T. Langen, R. Geiger, M. Kuhnert, B. Rauer, J. Schmiedmayer, *Nat. Phys.* **9**, 640–643 (2013).
22. D. S. Petrov, G. V. Shlyapnikov, J. T. M. Walraven, *Phys. Rev. Lett.* **85**, 3745–3749 (2000).
23. J. Reichel, V. Vuletic, Eds., *Atom Chips* (Wiley-VCH, Berlin, 2011).
24. T. Schumm *et al.*, *Nat. Phys.* **1**, 57–62 (2005).
25. See supplementary materials on *Science* Online.
26. T. Betz *et al.*, *Phys. Rev. Lett.* **106**, 020407 (2011).
27. J. Berges, S. Borsányi, C. Wetterich, *Phys. Rev. Lett.* **93**, 142002 (2004).
28. T. Gasenzer, J. Berges, M. G. Schmidt, M. Seco, *Phys. Rev. A* **72**, 063604 (2005).
29. J. Berges, T. Gasenzer, *Phys. Rev. A* **76**, 033604 (2007).
30. M. Eckstein, M. Kollar, P. Werner, *Phys. Rev. Lett.* **103**, 056403 (2009).
31. T. Kitagawa, A. Imambekov, J. Schmiedmayer, E. Demler, *New J. Phys.* **13**, 073018 (2011).
32. R. Bistritzer, E. Altman, *Proc. Natl. Acad. Sci. U.S.A.* **104**, 9955–9959 (2007).
33. T. Kitagawa *et al.*, *Phys. Rev. Lett.* **104**, 255302 (2010).
34. P. Barmettler, C. Kollath, http://arxiv.org/abs/1312.5757 (2013).
35. I. G. Hughes, T. Hase, *Measurements and Their Uncertainties* (Oxford Univ. Press, Oxford, 2010).
36. R. Hübener, A. Mari, J. Eisert, *Phys. Rev. Lett.* **110**, 040401 (2013).
37. T. Berrada *et al.*, *Nat. Commun.* **4**, 2077 (2013).

ACKNOWLEDGMENTS

We acknowledge discussions with E. Demler, E. Dalla Torre, K. Agarwal, J. Berges, M. Karl, V. Kasper, I. Bouchoule, M. Cheneau, and P. Grisins. Supported by the European Union (SIQS and ERC advanced grant QuantumRelax), the Austrian Science Fund (FWF) through the Doctoral Programme CoQuS (W1210) (B.R. and T.S.), the Lise Meitner Programme M1423 (R.G.) and project P22590-N16 (I.E.M.), Deutsche Forschungsgemeinschaft grant GA677/7,8 (T.G.), the University of Heidelberg Center for Quantum Dynamics, Helmholtz Association grant HA216/EMMI, and NSF grant PHY11-25915. T.L., T.G., and J.S. thank the Kavli Institute for Theoretical Physics, Santa Barbara, for its hospitality.

SUPPLEMENTARY MATERIALS

www.sciencemag.org/content/348/6231/207/suppl/DC1
Materials and Methods
Supplementary Text
References (*38*–*44*)

5 June 2014; accepted 2 March 2015
10.1126/science.1257026

BIOANALYSIS

Mass spectrometry imaging with laser-induced postionization

Jens Soltwisch,[1] Hans Kettling,[1,2] Simeon Vens-Cappell,[1,2] Marcel Wiegelmann,[1] Johannes Müthing,[1] Klaus Dreisewerd[1,2]*

Matrix-assisted laser desorption/ionization mass spectrometry imaging (MALDI-MSI) can simultaneously record the lateral distribution of numerous biomolecules in tissue slices, but its sensitivity is restricted by limited ionization. We used a wavelength-tunable postionization laser to initiate secondary MALDI-like ionization processes in the gas phase. In this way, we could increase the ion yields for numerous lipid classes, liposoluble vitamins, and saccharides, imaged in animal and plant tissue with a 5-micrometer-wide laser spot, by up to two orders of magnitude. Critical parameters for initiation of the secondary ionization processes are pressure of the cooling gas in the ion source, laser wavelength, pulse energy, and delay between the two laser pulses. The technology could enable sensitive MALDI-MS imaging with a lateral resolution in the low micrometer range.

Matrix-assisted laser desorption/ionization mass spectrometry (MALDI-MS) is used for the analysis of large nonvolatile biomolecules (*1*). Typically, the analytes are embedded into crystalline MALDI matrices (often aromatic carboxylic acids). Laser-induced codesorption of both constituents into the gas phase is convoluted with concomitant ionization in primary and secondary ionization processes (*2*–*4*). MALDI-MS imaging (MALDI-MSI) visualizes the lateral distribution of numerous biomolecules or that of administered drugs simultaneously by scanning matrix-coated tissue slices with a finely focused laser beam and recording the ion profiles per irradiated pixel (*5*, *6*). For

[1]Institute for Hygiene, University of Münster, Robert-Koch-Strasse 41, 48149 Münster, Germany. [2]Interdisciplinary Center for Clinical Research (IZKF), University of Münster, Domagkstrasse 3, 48149 Münster, Germany.
*Corresponding author. E-mail: klaus.dreisewerd@uni-muenster.de

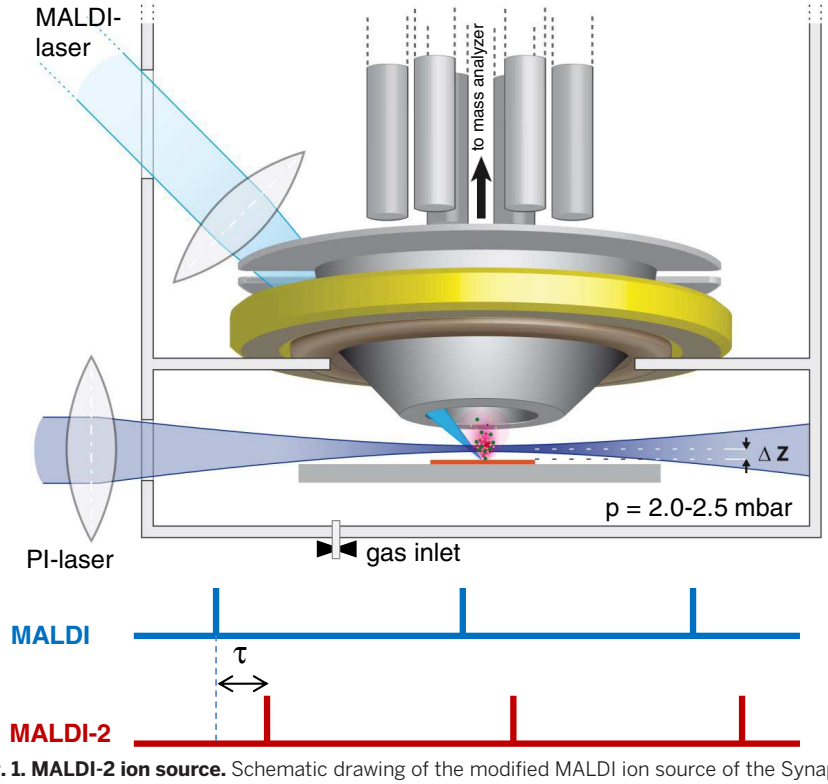

Fig. 1. MALDI-2 ion source. Schematic drawing of the modified MALDI ion source of the Synapt G2-S mass spectrometer with primary MALDI and PI laser beams and shielding aperture for increasing the cooling gas pressure in the region of ion generation; 2.0 to 2.5 mbar of N_2 were used for the MALDI-2-MSI measurements. The lower panel illustrates the laser pulse triggering sequence.

Experimental observation of a generalized Gibbs ensemble

Tim Langen, Sebastian Erne, Remi Geiger, Bernhard Rauer, Thomas Schweigler, Maximilian Kuhnert, Wolfgang Rohringer, Igor E. Mazets, Thomas Gasenzer and Jörg Schmiedmayer

Science **348** (6231), 207-211.
DOI: 10.1126/science.1257026

Detecting multiple temperatures

Most people have an intuitive understanding of temperature. In the context of statistical mechanics, the higher the temperature, the more a system is removed from its lowest energy state. Things become more complicated in a nonequilibrium system governed by quantum mechanics and constrained by several conserved quantities. Langen *et al.* showed that as many as 10 temperature-like parameters are necessary to describe the steady state of a one-dimensional gas of Rb atoms that was split into two in a particular way (see the Perspective by Spielman).

Science, this issue p. 207; see also p. 185

Science (print ISSN 0036-8075; online ISSN 1095-9203) is published by the American Association for the Advancement of Science, 1200 New York Avenue NW, Washington, DC 20005. The title *Science* is a registered trademark of AAAS.